Comparative Hall studies in the electron- and hole-doped manganites $La_{0.33}Ca_{0.67}MnO_3$ and $La_{0.70}Ca_{0.30}MnO_3$

I. Gordon, P. Wagner, A. Das, J. Vanacken, V. V. Moshchalkov, and Y. Bruynseraede
Laboratorium voor Vaste-Stoffysica en Magnetisme, Katholieke Universiteit Leuven, Celestijnenlaan 200D, 3001 Leuven, Belgium

W. Schuddinck and G. Van Tendeloo
EMAT, University of Antwerp (RUCA), Groenenborgerlaan 171, B-2020 Antwerpen, Belgium

M. Ziese
Department of Superconductivity and Magnetism, Institut für Experimentalphysik II, Universität Leipzig, Linnéstrasse 5, D-04103 Leipzig, Germany

G. Borghs
IMEC, Kapeldreef 75, 3001 Leuven, Belgium
(Received 8 June 2000)

A comparative study of the Hall effect and the longitudinal resistivity of $La_{1-x}Ca_xMnO_3$ ($x=0.30$ and $x=0.67$) thin films has been performed. The underdoped samples ($x=0.30$) show a semiconductor-to-quasimetal transition, and a colossal magnetoresistance (CMR) effect around $T_C=280$ K. The samples with $x=0.67$ stay semiconducting at low temperatures, and show a CMR effect up to 99% in magnetic fields of 50 T. In both compounds an extraordinary Hall contribution was found, with opposite sign to the regular Hall effect. For $x=0.30$ the charge carriers are hole-type, whereas for $x=0.67$ we observe electron-type carriers. The extraordinary Hall coefficient R_A can be linked to the longitudinal resistivity ρ_{xx} via $R_A \propto \rho_{xx}^{\alpha}$ with $\alpha=1.38$ for $x=0.30$, and $\alpha=0.60$ for $x=0.67$.

I. INTRODUCTION

Since the discovery of colossal magnetoresistance (CMR) in $La_{1-x}Ca_xMnO_3$ (LCMO) and related rare-earth manganese perovskites,[1] considerable effort has been devoted to the research of these compounds. The partial substitution of La^{3+} by Ca^{2+} introduces a mixture of Mn^{3+} and Mn^{4+} ions. Both Mn ions have three electrons in the t_{2g} state forming a localized $S=3/2$ spin, and Mn^{3+} has one extra electron in the e_g state, which can hop between nearest-neighbor Mn ions. The magnetic and electronic properties of manganites arise from the strong coupling between these correlated, itinerant e_g electrons and the localized spins. The double exchange mechanism (DE) between Mn^{3+} and Mn^{4+} is essential in order to understand the electric conduction.[2–4] In this model the e_g electron can hop to a neighboring Mn^{4+} ion with an effective hopping integral of the form $t=t_0\cos(\theta/2)$, where t_0 is the transfer integral when all spins are aligned, depending on the spatial wave functions, and θ is the angle between the spins of the Mn ions. Recently it was shown that DE alone is not enough to explain all magnetotransport properties, and that spin correlations and the coupling of carriers to the lattice and its distortions must be taken into account.[5,6] A CMR description is also possible in the framework of the spin dependent hopping model.[7] The hopping barrier of the e_g electrons is controlled by the relative spin misorientation at the hopping sites, and is considerably reduced due to the spin alignment induced by internal or external fields. A general overview of the literature on doped manganese oxides can be found in Refs. 8 and 9.

By changing the doping level x in the $La_{1-x}Ca_xMnO_3$ series, a rich phase diagram is obtained:[10] For $x\lesssim 0.15$ the samples are insulating at all temperatures, and charge and orbital ordering appear. The ground state is either a canted ferromagnet or antiferromagnet. When $0.15\lesssim x\lesssim 0.50$ the samples show a transition from a paramagnetic (PM) - semiconducting to a ferromagnetic (FM) - quasimetallic state. In this doping regime the CMR effect is most pronounced around the Curie temperature T_C, with a maximum for $x\approx 1/3$. Finally, when the samples are overdoped ($x\gtrsim 0.50$), the ground state becomes an insulating antiferromagnet. In these compounds it is suggested that charge-ordering suppresses ferromagnetism, allowing the system to enter an antiferromagnetic (AFM) state.[10]

The relation between these nominal doping levels and the resulting properties of charge carriers, like type, concentration, and mobility, is still not entirely resolved. Hall experiments on thin films of the intermediate doping level $x\approx 0.50$ point out that the carriers are holes with a concentration corresponding to the chemical substitution.[11,12] In the underdoped regime ($x<0.50$), Hall measurements have been performed on both thin films[13–19] and single crystals.[20,21] They all suggest hole-type carriers as well, but with indications for compensation effects since the apparent hole densities are by far larger than expected from the doping concentration. Finally the smaller bandfilling of overdoped manganites ($x>0.50$) has an influence on the electronic properties. In these samples electronlike carriers are expected, but no thorough investigation has been done up to now. Besides the normal Hall effect, the Hall signal in manganese perovskites contains generally an additional extraordinary contribution. This extraordinary (or anomalous) Hall effect is well known from observation in magnetic metals,[22] where it is caused by asymmetric skew and side jump scattering.[23] Frequently these mechanisms are also invoked

to explain the extraordinary Hall effect in the CMR manganites.[11–21]

In this article we compare the Hall effect and the negative magnetoresistivity of manganites with ''opposite'' chemical substitution. The underdoped $La_{0.70}Ca_{0.30}MnO_3$ has a majority of Mn^{3+} compared to Mn^{4+} and will in the following be denoted as ''*h*-LCMO'' to indicate the hole-type character of the resulting charge carriers. The overdoped $La_{0.33}Ca_{0.67}MnO_3$ contains a majority of Mn^{4+} and will be abbreviated as ''*e*-LCMO'' to account for the assumed electron-type character of the charge carriers. From the structural point of view these two materials have a comparable bond angle between adjacent Mn sites ($\Theta \approx 160°$). Therefore the difference in transport properties can be directly linked to the different bandfilling.

II. EXPERIMENTAL

Epitaxial thin films of $La_{1-x}Ca_xMnO_3$ with $x=0.30$ and $x=0.67$ were deposited onto $LaAlO_3$ (001) and $SrTiO_3$ (001) substrates by pulsed laser deposition from stoichiometric ceramic targets. The $La_{0.70}Ca_{0.30}MnO_3$ films were grown at 700 °C and postannealed for 2 h at 950 °C, as described in more detail in Ref. 24. The $La_{0.33}Ca_{0.67}MnO_3$ samples were deposited at temperatures around 850° C and post-annealed for 30 min at 830 °C. Epitaxial growth and correct lattice constants were verified for both compounds by x-ray diffraction. All films were single phased, and showed rocking curves with a full width at half maximum below 0.35°. The average lattice constants were (3.85 ± 0.02) Å for *h*-LCMO, and (3.77 ± 0.02) Å for *e*-LCMO, in agreement with literature values.[25] The Rutherford backscattering (RBS) composition analysis showed that all films had the correct nominal stoichiometry with an error less than 5%. The thickness of the films was between 1500 Å and 2400 Å, which was determined by RBS and atomic force microscopy.

Since the lattice mismatch between film and substrate is apparently large for *e*-LCMO we also performed transmission electron microscopy (TEM) to check whether there are abundant defect structures, which might mask the intrinsic transport properties. The TEM samples in cross-section geometry were cut parallel to the $\langle 001 \rangle$ direction of $SrTiO_3$. Electron diffraction patterns, see Fig. 1(a), and high-resolution images like Fig. 1(b) were obtained using a JEOL 4000 EX microscope operating at 400 kV with a resolution of 1.7 Å. All diffraction patterns could be indexed in an orthorhombic, *Pnma*-type unit cell with the lattice parameters $a_o \approx b_o \approx 5.4$ Å ($\approx \sqrt{2} \times a_p$) and $b_o \approx 7.6$ Å ($\approx 2 \times a_p$). The indices *o* and *p* refer to the orthorhombic and to the pseudocubic cell representation. The diffraction pattern along $[101]_o$ (i.e., the film's normal axis) in Fig. 1(a) is a superposition of the film and the substrate.

The higher order reflections show a doublet splitting along b_0^* meaning that the film is relaxed in the direction perpendicular on the substrate, with the substrate's lattice parameter being 2.2% larger than that of the film. High-resolution TEM images show that twinning and grain boundaries, typical features of *Pnma*-type crystals, are both absent in these samples. Nevertheless, there are pseudoperiodic growth defects at the film-substrate interface, which could be identified as epitaxial misfit dislocations with a mutual distance of 200–300 Å. An individial dislocation is magnified in Fig. 1(b): the strain field of the dislocation extends into the film on a scale of 100–150 Å and relaxes above this length scale. The very particular strain field and the bending of the lattice planes is most probably due to the adsorbtion of foreign atoms around the dislocation core. Keeping in mind that the samples used for Hall measurements are typically 2000 Å thick, we conclude that the transport properties will not be seriously affected by these defect structures.

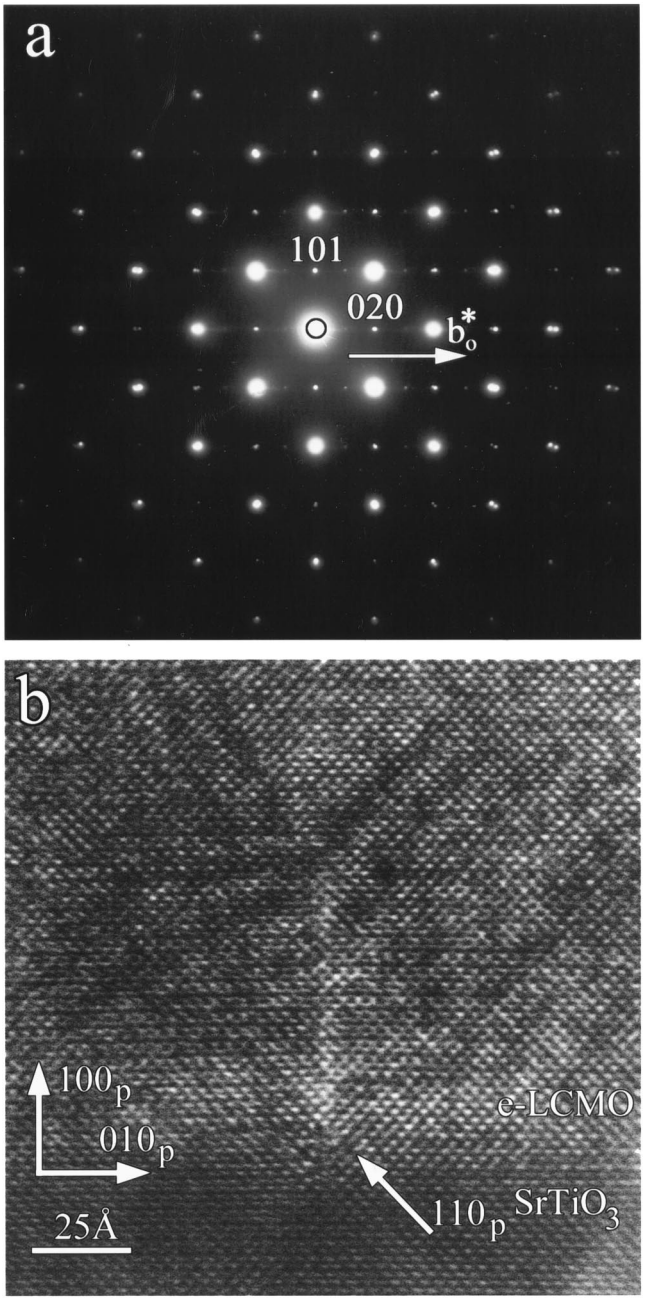

FIG. 1. (a) Electron diffraction pattern of *e*-LCMO along the $[101]_o$ direction, i.e., the axis perpendicular on the film surface. Higher order spots are slightly split due to the small difference in the lattice parameters of *e*-LCMO and $SrTiO_3$. (b) High-resolution TEM image of a misfit-induced dislocation at the interface between the film and the substrate. The dislocation is oriented along the white arrow.

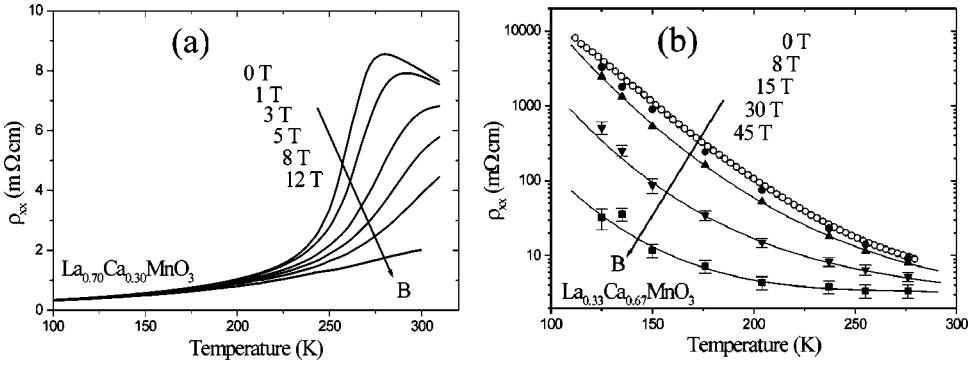

FIG. 2. Temperature dependence of the longitudinal resistivity ρ for (a) *h*-LCMO and (b) *e*-LCMO. In (a) the measurements are performed in persistent magnetic fields up to 12 T, while in (b) pulsed fields up to 50 T were used. All magnetic fields were applied perpendicular to the film surface. The solid lines in (b) are a guide to the eye.

To perform transport measurements, the films were patterned by standard methods into a four-point geometry with evaporated and annealed gold contacts. The longitudinal resistance and the Hall resistance were measured in a He-flow cryostat at constant temperatures and in fields up to 12 T (see Ref. 12). The Hall signal was calculated from the half difference of the transverse resistances, measured with the field oriented parallel and antiparallel to the films normal axis. For the transport studies at higher magnetic fields, the pulsed field setup described in Ref. 26 was employed. This allowed to measure the resistivity in fields up to 50 T at a time scale of 10–20 ms. All measurements were performed with the magnetic field perpendicular to the film surface.

III. COLOSSAL MAGNETORESISTANCE

The temperature dependence of the longitudinal resistivity ρ_{xx} in various magnetic fields is shown for *h*-LCMO in Fig. 2(a) and for *e*-LCMO in Fig. 2(b). The underdoped samples show a semiconductor to quasi-metal transition around 275 K, which is slightly below the Curie temperature $T_C = 280$ K, as determined by SQUID measurement. By applying a magnetic field the resistivity is lowered for temperatures in the vincinity of T_C, and the transition temperature is raised. Both effects contribute to the colossal negative magnetoresistance (CMR). At lower temperatures ($T < 150$ K) the CMR effect vanishes almost completely, which is a sign of good ferromagnetic ordering of the films.

Figure 2(b) shows the temperature dependent resistivity for *e*-LCMO in zero field and in pulsed magnetic fields. Although at room temperature *e*-LCMO has the same longitudinal resistivity as *h*-LCMO ($\rho_{xx} \approx 8$ mΩ cm), it stays insulating at lower temperatures, and does not show any electronic transition down to 100 K. Below 100 K, ρ_{xx} became too high to measure. The zero-field data could be fitted by Mott's variable-range hopping formula $\rho_{xx} \propto \exp(T_0/T)^{1/4}$, with $T_0 = 5.6 \times 10^6$ K. Other models like an Arrhenius law or nearest-neighbor hopping of small polarons,[24] are less adequate in describing the resistivity.

In contrast to *h*-LCMO, the *e*-LCMO films show almost no magnetoresistance in fields below 8 T. At higher magnetic fields ($B \gtrsim 15$ T) however, a considerable negative magnetoresistivity is found. At temperatures below 200 K and in fields of 45 T the samples become almost magnetically saturated, and a decrease in resistivity of $\Delta\rho/\rho_0 = (\rho_0 - \rho_B)/\rho_0 > 99\%$ is observed. But even at these high fields the samples still show a insulating behavior, and no trace of a transition to a quasimetallic state like in *h*-LCMO is seen. This is an indication that the total hopping barrier consists of different contributions:[7] the magnetic part vanishes under magnetic saturation, while the nonmagnetic contributions stay finite. For all investigated temperatures the decrease of ρ_{xx} as a function of field scales with the square of the magnetization-related Brillouin function $\mathcal{B}^2$, which explains the apparent absence of CMR in small fields.

IV. HALL EFFECT

The Hall resistivity in magnetic materials contains two contributions: the normal and the extraordinary Hall effect[22]

$$\rho_{xy}(B,T) = R_0(T) \cdot B + R_A(T) \cdot \mu_0 \cdot M(B,T), \qquad (1)$$

with R_0 the ordinary Hall coefficient, μ_0 the vacuum permeability, M the magnetization, and R_A the extraordinary Hall coefficient depending on temperature and not on the external magnetic field. In manganites this description is widely used.[11–21]

Figure 3(a) shows ρ_{xy} vs B for $La_{0.70}Ca_{0.30}MnO_3$, measured at temperatures between 10 K and 240 K. The total

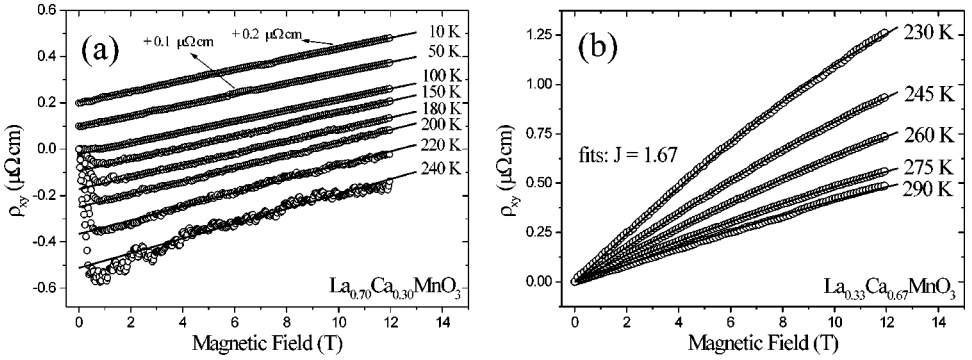

FIG. 3. Field dependence of the Hall resistivity ρ_{xy} at different temperatures for (a) *h*-LCMO and (b) *e*-LCMO. In both cases normal and extraordinary Hall contributions have opposite sign. In *h*-LCMO the normal Hall constant R_0 is positive (holes), whereas in *e*-LCMO R_0 is negative (electrons). The curves at 10 K and 50 K in (a) are shifted for clarity. The solid lines in (a) and (b) are fits to determine the carrier densities.

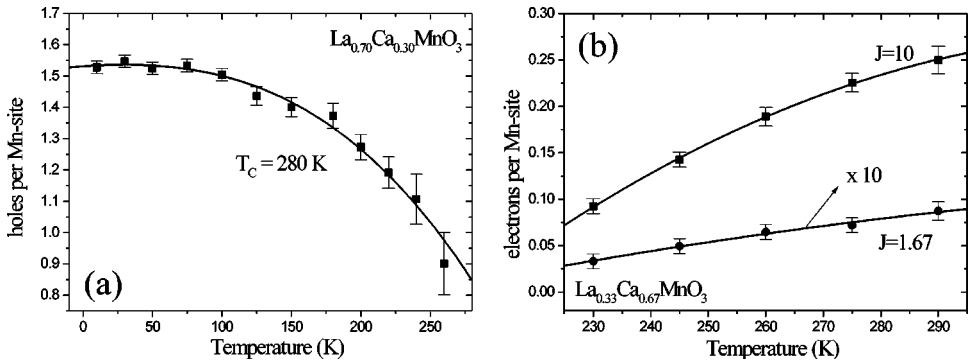

FIG. 4. Temperature dependence of the number of charge carriers for (a) *h*-LCMO and (b) *e*-LCMO. The solid lines are a guide to the eye. For *e*-LCMO the curves are obtained by using Eq. (2) for the fixed values $J=1.67$ and $J=10$.

transverse signal had a contribution of the longitudinal resistance due to imperfect alignment of the Hall contacts. Especially for temperatures around $T_C=270$ K, where the CMR effect is large, this caused an enhanced noise level, which made Hall measurements in the paramagnetic state impossible. At temperatures above 100 K the Hall signal is dominated at low fields by a steep electronlike decrease, attributed to the extraordinary Hall effect. At higher fields ρ_{xy} saturates, followed by a linear increase corresponding to the ordinary Hall effect. This behavior can be understood by applying Eq. (1): In the ferromagnetic state the magnetization M rises quickly and becomes saturated at sufficiently large fields of the order of several T. At low fields ρ_{xy} is therefore dominated by the extraordinary Hall effect, whereas the normal Hall effect dominates at higher fields. The solid lines in Fig. 3(a) are linear fits of the high-field data, which allow us to determine the hole-type carrier concentration from the respective slopes. For $T<100$ K the extraordinary Hall contribution to the Hall curves is negligible, indicating that $R_A \rightarrow 0$ at low temperatures.[11–15,18–20]

Figure 3(b) shows the field dependence of the Hall signal for $La_{0.33}Ca_{0.67}MnO_3$ at temperatures between 230 K and 290 K. Also in these samples a longitudinal contribution to ρ_{xy} was encountered, and because of the insulating behavior [see Fig. 2(b)], quantitative data below 230 K could not be obtained. For all investigated temperatures the Hall curves have a positive slope over the available field range, but are neither linear, nor proportional to the magnetization. Therefore we assume that like in *h*-LCMO, the Hall signal of *e*-LCMO consists of two different contributions [see Eq. (1)]. Since the samples are paramagnetic or superparamagnetic in the investigated temperature range,[10] the magnetization M scales with the Brillouin function $\mathcal{B}(J,B,T)$,[27,28] and Eq. (1) can be rewritten as

$$\rho_{xy}=R_0\cdot B+R_A\cdot C\cdot \mathcal{B}\left(\frac{g\cdot\mu_B\cdot J\cdot B}{k_BT}\right), \qquad (2)$$

with $C=g\cdot\mu_0\cdot\mu_B\cdot\overline{J}/V_{\mathrm{cell}}$. The proportionality constant C contains the gyromagnetic ratio $g=2$, the vacuum permeability μ_0, the Bohr magneton μ_B, the unit cell volume V_{cell}, and the average spin per Mn site $\overline{J}=1.67$. The J factor in the argument of the Brillouin function is not known *a priori*, but we can estimate values for a lower and an upper bound. The lower limit is naturally $J=\overline{J}$, the upper limit is estimated as $J=10$. This moment corresponds to spin clusters consisting of roughly 6 Mn sites as determined for the medium-doped compound $Nd_{0.5}Sr_{0.5}MnO_3$ (NSMO), which shows short range ferromagnetic order (superparamagnetism) already in the PM phase.[7] Fitting the Hall data of Fig. 3(b) with Eq. (2) results for the lower and the upper limit of J in a negative R_0 and a positive R_A. The solid lines in Fig. 3(b) represent these fits for $J=1.67$, but fits with $J=10$ work equally well. This confirms that in the overdoped samples electronlike carriers are responsible for the charge transport. The same behavior—electron-type carriers and a positive extraordinary Hall effect—was also observed in the double-perovskite Sr_2FeMoO_6, and in iron and its alloys.[29,30]

A. Normal Hall contribution

From the R_0 values for both *h*-LCMO and *e*-LCMO the carrier density n can be calculated in a one-band model via $R_0=1/ne$. The results are shown in Figs. 4(a) (*h*-LCMO), and 4(b) (*e*-LCMO). The number of hole-type charge carriers per chemical unit cell n_h for $La_{0.70}Ca_{0.30}MnO_3$ decreases from 1.55 below 100 K to 0.90, close to T_C. Similar drops in carrier density near T_C were already observed in intermediate- and underdoped manganites before.[12,15,19,21] It could be the result of a change in conduction mechanism from hopping of localized polarons (low mobility) above T_C to metallic behavior via itinerant electrons (high mobility) below T_C.[31] As pointed out earlier,[12] n_h is field independent, and the CMR is caused by an increase in the carrier mobility μ_h. Around T_C μ_h goes from 7 mm^2/Vs at 0 T to 21 mm^2/Vs at 8 T. The obtained values for n_h are surprisingly high since from chemical doping a nominal value of 0.30 holes per Mn site is expected. Similar high values ($1<n_h<3$) are reported for other underdoped manganites,[11,14,15,18–20] and even values up to 7 are reported.[13] Jakob *et al.*[15] interpreted these high carrier densities within a two-band model. This interpretation is based on band structure calculations in $La_{0.67}Ca_{0.33}MnO_3$ by Pickett *et al.*[32] Their virtual-crystal approximation yields a Γ-centered spherical Fermi surface with $n_e=0.05$ electrons per unit cell, and a R-centered cubic Fermi surface containing $n_h=0.55$ holes per unit cell. These calculations were recently verified experimentally by Fermi surface measurements on $La_{0.70}Ca_{0.30}MnO_3$, using the two-dimensional angular correlation of electron-positron annihilation radiation (2D-ACAR) technique.[33] The relation between the Hall coefficient R_0 and the number of carriers in a two-band system is:[15]

$$R_0=\frac{n_h\mu_h^2-n_e\mu_e^2}{e(n_h\mu_h+n_e\mu_e)^2}=\frac{n_h-n_e\mu^{*2}}{e(n_h+n_e\mu^*)^2}. \qquad (3)$$

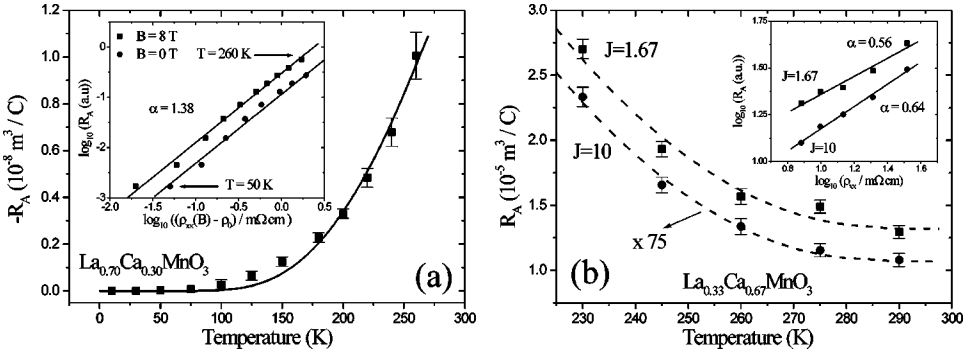

FIG. 5. (a) Temperature dependence of the extraordinary Hall coefficient R_A for *h*-LCMO. The solid line is a fit according to the theory of Ye *et al.*[34] R_A is linked to the longitudinal resistivity ρ_{xx} (at 0 T and 8 T) via $R_A \propto (\rho_{xx}-\rho_0)^{\alpha}$ with $\alpha = 1.38$ (see inset). (b) Temperature dependence of R_A for *e*-LCMO, calculated from Eq. (2) with different J values (dashed lines are guides to the eye). R_A scales with the zero-field resistivity via $R_A \propto \rho_{xx}^{\alpha}$ with $\alpha = (0.60 \pm 0.05)$ (see inset).

From Eq. (3) the mobility ratio between holes and electrons $\mu^* = \mu_e/\mu_h$ can be estimated. Below 100 K this gives $\mu^* = 2.3$, and this decreases with increasing temperature to $\mu^* = 1.58$ at 260 K. From the density of states at the Fermi level, given in Ref. 32, an effective mass ratio for holes and electrons of $m_h^*/m_e^* \approx 2.0$ can be calculated.[15] If equal mean-free paths $l_h = l_e$ are assumed, this ratio together with the slightly different Fermi velocities at the 2 Fermi surfaces [$v_F(e) = 7.1 \times 10^5$ m/sec and $v_F(h) = 7.6 \times 10^5$ m/sec[32]], gives a mobility ratio $x = 2.15$, corresponding very well to the experimental low-temperature value.

From fitting the Hall data of *e*-LCMO [see Fig. 3(b)] with Eq. (2), we get R_0 for J between the lower ($J = 1.67$) and upper ($J = 10$) limits. Regardless of the choice of J we always obtain the same features: electron-type charge carriers, and a decreasing carrier density n_e with decreasing temperature. This behavior is expected for a semiconductor in which not only the carrier mobility but also the carrier density is thermally activated. At room temperature n_e is between 0.009 ($J = 1.67$) and 0.250 ($J = 10$) electrons per chemical unit cell. At 230 K this decreases to $n_e \approx 0.003$ for $J = 1.67$, and $n_e \approx 0.092$ for $J = 10$. From chemical doping we would expect $n_e = 0.33$, assuming that all carriers are activated into the conduction band. At 260 K, where the longitudinal resistivity of *e*-LCMO is comparable to that of *h*-LCMO, the zero-field mobility of the electrons is $\mu_e = 379$ mm^2/Vs for $J = 1.67$, and $\mu_e = 13$ mm^2/Vs for $J = 10$. In both cases this is larger than the mobility of the holes in *h*-LCMO ($\mu_h = 7$ mm^2/Vs).

B. Extraordinary Hall contribution

For both compounds R_A can be extracted from the Hall data, allowing us to study the extraordinary Hall effect, which gives additional information about the transport properties. For *h*-LCMO R_A can be calculated from the spontaneous Hall effect $\rho_{xy}^* = \mu_0 \cdot M_S \cdot R_A$ if the saturated magnetization M_S is known.[12] ρ_{xy}^* is obtained from the intersection of the linear extrapolation of $\rho_{xy}(B)$ at high fields with the ρ_{xy} axis. M_S is calculated by assuming that in the saturated state all Mn spins are aligned parallel. This gives a value of $M_S \approx 6.0 \times 10^5$ A/m. The temperature dependence of R_A is shown in Fig. 5(a). Below T_C R_A decreases rapidly and vanishes at the lowest temperatures, in agreement with literature data.[12,14,15,18–20] Furthermore R_A is found to scale with the longitudinal resistivity ρ_{xx} via $R_A \propto \rho_{xx}^{\alpha}$. This power law normally yields α values between 1 (skew-scattering) and 2 (side-jumps).[12,15,18] It is the result of magnetic scattering processes which are responsible for both longitudinal resistivity, and extraordinary Hall effect through asymmetric spin-orbit coupling. According to Ref. 12 the scattering events without left-right asymmetry (lattice distortions, domain walls) should be discarded when checking the power law dependence. This is done by substracting ρ_0, the field-independent resistivity value in the limit $T \to 0$, from the total resistivity ρ_{xx}. The inset of Fig. 5(a) shows R_A for *h*-LCMO in comparison to the corrected ρ_{xx} values at 0 T and 8 T. In both cases the power law is valid with $\alpha = 1.38$, in between the values for skew- and side jump scattering.

The extraordinary Hall constant R_A of *e*-LCMO can be calculated by fitting the Hall data with Eq. (2). Although the absolute value of R_A depends on J, the physical behavior is J independent, and R_A increases with decreasing temperature [see Fig. 5(b)]. At room temperature R_A ranges from $R_A = 14.4 \times 10^{-8}$ m^3/C ($J = 10$) to $R_A = 1.30 \times 10^{-5}$ m^3/C ($J = 1.67$). These values are unexpectedly high compared to *h*-LCMO [Fig. 5(a)]. The inset shows R_A as a function of the zero-field resistivity ρ_{xx} for both J values, and the scaling law $R_A \propto \rho_{xx}^{\alpha}$ is valid with $\alpha = (0.60 \pm 0.05)$. This exponent is much smaller than that of *h*-LCMO, and clearly below the value for skew scattering ($\alpha = 1$). These deviations (exponent and absolute R_A value) could be expected since skew scattering is *a priori* not applicable to hopping-type charge transport. A similarly low exponent ($\alpha = 0.75$) was also obtained for semiconducting samples of the double-perovskite Sr_2FeMoO_6 (SFMO).[29]

A theory which might be suitable to explain the extraordinary Hall effect in CMR manganites has been developed recently.[34] It is based on the so-called Berry phase, which electrons acquire when moving from site to site in a topologically nontrivial background of localized spin moments (skyrmions). Under the influence of the spin-orbit interaction this phase leads to an extraordinary Hall contribution with opposite sign between R_A and R_0, which cannot be explained in a straightforward way by skew- and side jump scattering. Furthermore, the model makes specific predictions for the temperature dependence of R_A. At temperatures

below T_C an activated behavior, resulting from the exponential suppressing of the skyrmion density at low T, is expected according to $R_A \sim e^{-E_C/k_B T}$. Applying this formula to the *h*-LCMO data gives a convincing fit with $E_C = 78$ meV [see Fig. 5(a)]. In the paramagnetic phase strong thermal spin fluctuations disrupt local correlations and according to the model, R_A should decrease with the power law $R_A \sim 1/T^3$. A decrease is clearly visible in the *e*-LCMO data [see Fig. 5(b)], but convincing agreement with the T^{-3} law could not be found.

V. CONCLUSIONS AND SUMMARY

We investigated magnetoresistance and Hall effect in $La_{1-x}Ca_xMnO_3$ for $x=0.30$ and $x=0.67$. A colossal negative magnetoresistance effect was found in both compounds, but on different field scales. The *e*-LCMO samples stayed semiconducting even in fields up to 50 T, and no transition to a quasimetallic state was observed. The *h*-LCMO films yielded hole-type charges with a carrier density $n_h \approx 1.55$ at low temperatures. This indicates a compensation effect which was quantitatively explained in a two-band model. As expected from bandfilling, the *e*-LCMO samples showed an electronlike normal Hall effect. We estimated the number of electrons per unit cell of *e*-LCMO to be between 0.009 and 0.25. The extraordinary Hall effect has for both compounds the opposite sign of the normal Hall contribution. Furthermore, the anomalous Hall coefficient scales with the longitudinal resistivity according to $R_A \propto \rho_{xx}^{\alpha}$ with $\alpha = 1.38$ for *h*-LCMO and $\alpha = 0.60$ for *e*-LCMO. The exponent of 1.38 in case of *h*-LCMO points to the presence of asymmetric scattering mechanisms — but the data [especially $R_A(T)$] can be explained equally well within Ye's Berry-phase model. Therefore, we cannot draw a conclusive decision about the validity of both explanations at the moment. The anomalous Hall effect in electron-doped *e*-LCMO can in principle not emerge from skew scattering and the temperature dependence of R_A is in qualitative agreement with the predictions of Ye and co-workers.

ACKNOWLEDGMENTS

This work was supported by the Flemish Concerted Action (GOA), the Fund for Scientific Research–Flanders (FWO), and the Belgian Interuniversity Attraction Poles programs (IUAP). A. D. acknowledges financial support by the Research Council of the Katholieke Universiteit Leuven. The authors thank K. Ruan, A. Vantomme, and F.G. Aliev.

[1] R.M. Kusters, J. Singleton, D.A. Keen, R. McGreevy, and W. Hayes, Physica B **155**, 362 (1989); R. von Helmolt, J. Wecker, B. Holtzapfel, L. Schultz, and K. Samwer, Phys. Rev. Lett. **71**, 2331 (1993).
[2] C. Zener, Phys. Rev. **82**, 403 (1951).
[3] P.W. Anderson and H. Hasegawa, Phys. Rev. **100**, 545 (1955).
[4] P.-G. de Gennes, Phys. Rev. **118**, 141 (1960).
[5] A.J. Millis, B.I. Shraiman, and R. Mueller, Phys. Rev. Lett. **77**, 175 (1996); A.J. Millis, R. Mueller, and B.I. Shraiman, Phys. Rev. B **54**, 5405 (1996).
[6] H. Röder, J. Zang, and A.R. Bishop, Phys. Rev. Lett. **76**, 1356 (1996); J. Zang, A.R. Bishop, and H. Röder, Phys. Rev. B **53**, R8840 (1996).
[7] P. Wagner, I. Gordon, L. Trappeniers, J. Vanacken, F. Herlach, V.V. Moshchalkov, and Y. Bruynseraede, Phys. Rev. Lett. **81**, 3980 (1998).
[8] A.P. Ramirez, J. Phys.: Condens. Matter **9**, 8171 (1997).
[9] J.M.D. Coey, M. Viret, and S. von Molnar, Adv. Phys. **48**, 167 (1999).
[10] P. Schiffer, A.P. Ramirez, W. Bao, and S.-W. Cheong, Phys. Rev. Lett. **75**, 3336 (1995).
[11] P. Wagner, D. Mazilu, L. Trappeniers, V.V. Moshchalkov, and Y. Bruynseraede, Phys. Rev. B **55**, R14 721 (1997).
[12] P. Wagner, I. Gordon, A. Vantomme, D. Dierickx, M.J. Van Bael, V.V. Moshchalkov, and Y. Bruynseraede, Europhys. Lett. **41**, 49 (1998).
[13] R. von Helmolt, in *Magnetowiderstandseffekte in heterogenen Legierungen und magnetischen Oxiden* (VDI-Verlag GmbH, Düsseldorf, 1995).
[14] P. Matl, N.P. Ong, Y.F. Yan, Y.Q. Li, D. Studebaker, T. Baum, and G. Doubinina, Phys. Rev. B **57**, 10 248 (1998).
[15] G. Jakob, F. Martin, W. Westerburg, and H. Adrian, Phys. Rev. B **57**, 10 252 (1998).
[16] P. Mandal, K. Bärner, L. Haupt, A. Poddar, R. von Helmolt, A.G.M. Jansen, and P. Wyder, Phys. Rev. B **57**, 10 256 (1998).
[17] C. Mitze, C. Osthöver, F. Voges, U. Hasenkox, R. Waser, and R.R. Arons, Solid State Commun. **109**, 189 (1999).
[18] M. Ziese and C. Srinitiwarawong, Europhys. Lett. **45**, 256 (1999).
[19] W. Westerburg, F. Martin, P.J.M. van Bentum, J.A.A.J. Perenboom, and G. Jakob, Eur. Phys. J. B **14**, 509 (2000).
[20] A. Asamitsu and Y. Tokura, Phys. Rev. B **58**, 47 (1998).
[21] S.H. Chun, M.B. Salomon, and P.D. Han, Phys. Rev. B **59**, 11 155 (1999).
[22] R. Karplus and J.M. Luttinger, Phys. Rev. **55**, 1154 (1954).
[23] L. Berger, Phys. Rev. B **2**, 4559 (1970).
[24] M. Ziese and C. Srinitiwarawong, Phys. Rev. B **58**, 11 519 (1998).
[25] J.F. Lawler, J.M.D. Coey, J.G. Lunney, and V. Skumryev, J. Phys.: Condens. Matter **8**, 10 737 (1996).
[26] F. Herlach, C.C. Agosta, R. Bogaerts, W. Boon, I. Deckers, A. De Keyzer, N. Harrison, A. Lagutin, L. Li, L. Trappeniers, J. Vanacken, L. Van Bockstal, and A. Van Esch, Physica B **216**, 161 (1996).
[27] N. W. Ashcroft and N. D. Mermin, *Solid State Physics* (Saunders College, Philadelphia, 1976).
[28] P. Wagner, I. Gordon, S. Mangin, V.V. Moshchalkov, Y. Bruynseraede, L. Pinsard, and A. Revcolevschi, Phys. Rev. B **61**, 529 (2000).
[29] W. Westerburg, F. Martin, and G. Jakob, J. Appl. Phys. **87**, 5040 (2000); W. Westerburg, D. Reisinger, and G. Jakob, Phys. Rev. B **62**, R767 (2000).
[30] G. Bergmann, Phys. Today **32** (8), 25 (1979).
[31] M. Jaime, P. Lin, S.H. Chun, M.B. Salamon, P. Dorsey, and M. Rubinstein, Phys. Rev. B **60**, 1028 (1999).
[32] W. E Pickett and D.J. Singh, Phys. Rev. B **55**, R8642 (1997).
[33] E.A. Livesay, R.N. West, S.B. Dugdale, G. Santi, and T. Jarlborg, J. Phys.: Condens. Matter **11**, L279 (1999).
[34] J. Ye, Y.B. Kim, A.J. Millis, B.I. Shraiman, P. Majumdar, and Z. Tešanović, Phys. Rev. B **83**, 3737 (1999).